Experimental investigations of flow field around hypersonic vehicle and re-entering spacecraft with the hypersonic rarefied wind tunnel MARHy

Romain Joussot[*][†], *Théo Gravalon*[*], *Nicolas Rembaut*[*] *and Viviana Lago*[*]
[*]*CNRS, ICARE, UPR 3021*
1C avenue de la Recherche Scientifique
CS 50060
F-45071, Orléans cedex 2, France
romain.joussot@cnrs-orleans.fr · theo.gravalon@cnrs-orleans.fr · nicolas.rembaut@cnrs-orleans.fr
viviana.lago@cnrs-orleans.fr
[†]Corresponding author

Abstract

This paper presents experimental investigations focused on flow field characterization around different geometries in high speed flows in the slightly rarefied regime: simplified models of CubeSat, a simplified model of Tiangong-1, and a model similar to the IXV. Experiments were performed in the MARHy wind tunnel, which can simulate most of the re-entry corridors from 100 km to 60 km of altitude. For the present study, models were tested in a Mach 4 flow (equivalent altitude of 68 km). For the CubeSat and the Tiangong-1 models, influence of the solar panels on the flow field was investigated.

1. Introduction

This paper presents experimental investigations focused on flow field characterization around different geometries in high speed flows in the slightly rarefied regime (or slip-flow regime). The model geometries tested in the wind tunnel were: simplified models of CubeSat (1U-, 2U- and 3U-configuration), a simplified model of the Chinese space station Tiangong-1, and a model similar to the IXV. The experiments were performed in the MARHy wind tunnel, which can be equipped with a wide range of nozzles, simulating most of the re-entry vehicles flight corridors from 100 km to 60 km of altitude. For the present study, models were tested in a Mach 4 flow with a free stream pressure of 8 Pa (equivalent altitude of about 68 km). The flow around the model was visualized with a CMOS camera and due to the rarefaction level of the flow, the flow field around the model was experimentally visualized with the glow-discharge flow visualization technique. An infrared thermography device was used to measure the surface temperature of each model during experiments. For the CubeSat and the Tiangong-1 models, influence of the solar panels on the flow field was investigated. In addition, several positions were tested to reproduce different initial conditions of satellite attitude at the beginning of the re-entry. For the IXV-like model, several angle of attack were tested.

2. Experimental setup

2.1 The MARHy wind tunnel

The experimental measurements were carried out in the MARHy wind tunnel (formerly known as the SR3 wind tunnel of the "Laboratoire d'Aérothermique"), which is one of the three wind tunnels of the FAST platform[3] of ICARE (CNRS, France). Three main parts compose this wind tunnel (Fig. 1): a settling chamber (for the stagnation conditions), a test chamber in which the measurements are performed (at free stream conditions), and a third chamber in which a diffuser is installed. The diffuser is connected to a powerful pumping group (total capacity of $153\,000\,\mathrm{m^3\,h^{-1}}$), which ensures the low density flow conditions in continuous operating mode. The settling chamber is connected to the test chamber through: a calibrated diaphragm for the subsonic flow conditions, a contoured de Laval nozzle for the supersonic flow conditions, or a conical nozzle for the hypersonic flow conditions. In the case of subsonic or supersonic

cases, the working gas was air of the experiment room. Molecular nitrogen N_2 is used in the case of hypersonic flow conditions.
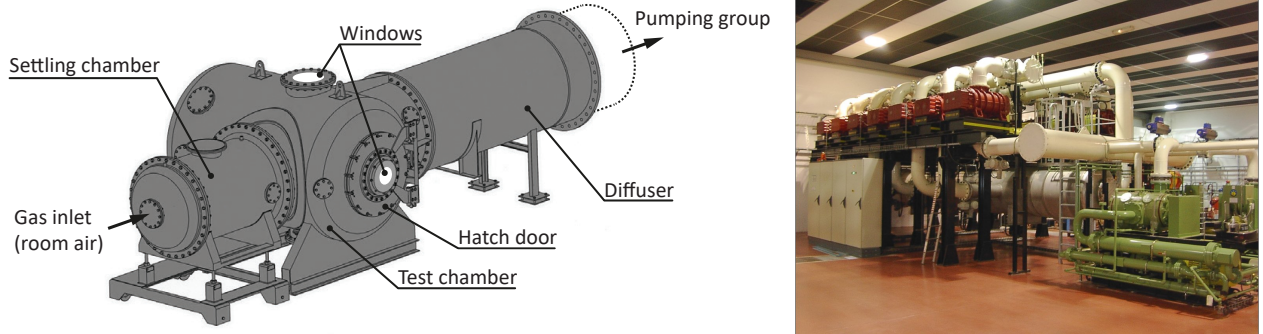

Figure 1: Hypersonic rarefied wind tunnel MARHy: schematic of the wind tunnel (left panel), and picture of the pumping group (right panel).

2.2 Flow conditions

The MARHy wind tunnel can be equipped with different nozzles to reproduce experimentally several flow conditions encountered during the re-entry of various geometries. A set of more than 20 nozzles is available and allows to test subsonic flows (Mach 0.6 and 0.8), supersonic ones (Mach 2 and 4), and hypersonic ones (from Mach 6.8 up to 30). The nominal operating conditions used for the present study corresponds to a supersonic flow at Mach 4 with a free stream pressure of 8.0 Pa. The conditions are detailed in Tab. 1, where the subscripts $_0$ and $_\infty$ stand for the stagnation conditions and the free stream ones, respectively.

Table 1: Flow conditions for the "Mach 4 – 8 Pa" nozzle (air as working gas).

Stagnation conditions	Free stream conditions
$p_0 = 1214.39$ Pa	$p_\infty = 8.00$ Pa
$T_0 = 293$ K	$T_\infty = 69.76$ K
$\rho_0 = 1.44 \times 10^{-2}$ kg m^{-3}	$\rho_\infty = 4.00 \times 10^{-4}$ kg m^{-3}
	$\mu_\infty = 1.108 \times 10^{-5}$ Pa s
	$U_\infty = 669.61$ m s^{-1}
	$Ma_\infty = 4.0$
	$\lambda_\infty = 0.106$ mm

For the present study, the static pressure p_∞ in the test chamber corresponds to a geometric altitude of 68 km in considering the Naval Research Laboratory Mass Spectrometer and Incoherent Scatter Radar Exosphere (NRLMSISE-00) model,[4] which was used to simulate the atmospheric properties (temperature, pressure, and total number density) as a function of altitude. Figure 2 shows the flow conditions that can be tested with the MARHy wind tunnel in terms of free stream pressure and equivalent altitude (calculated with the NRLMSISE-00 model). One can see that most of these equivalent altitudes are close to the typical breakup altitudes (i.e., between 75 km and 85 km) that are usually set in re-entry codes.[1]

Figure 3 shows the flow conditions parametrized in terms of the Mach number (Ma), Reynolds number (Re_L), and Knudsen number (Kn_L), for the nozzles of the MARHy wind tunnel. In this study, the Knudsen number is defined as

$$Kn_L = \frac{\lambda}{L_{ref}}, \tag{1}$$

where λ is the mean free path (in m) and L_{ref} is a characteristic length (in m) of the problem. The mean free path for the free stream condition was estimated assuming a variable cross-section hard sphere (VHS) model as

$$\lambda_\infty = \frac{\mu_\infty}{\rho_\infty \sqrt{2R_m T_\infty}} \frac{2\,(7 - 2\omega)\,(5 - 2\omega)}{15\,\sqrt{\pi}}, \tag{2}$$
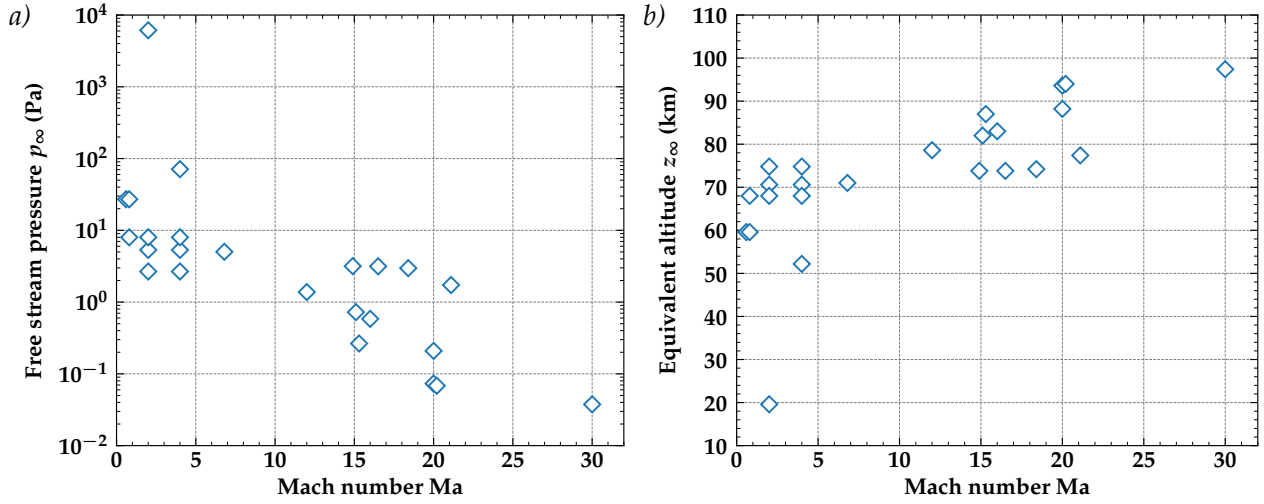
Figure 2: Flow conditions of the MARHy wind tunnel in terms of: *a)* free stream pressure, and *b)* equivalent altitude calculated with the NRLMSISE-00 model. Each point represents the flow condition of each available nozzle.

where μ_∞ is the dynamic viscosity (in Pa s) calculated with the Chapman-Enskog relation (Eq. 3), ρ_∞ is the total mass density in kg m^{-3}, Rm is the gas constant in J kg^{-1} K^{-1} ($R_m = 287.05$ J kg^{-1} K^{-1} for air), T_∞ is the temperature in K, and ω is the viscosity temperature exponent ($\mu \propto T^\omega$, Eq. 4). Even thought many other molecule interactions model exist, the VHS model is one of the most used in the literature due to its simple implementation. The dynamic viscosity was defined as

$$\mu = \frac{AT^{1.5}}{B + T},$$ (3)

where $A = 1.458 \times 10^{-6}$, and $B = 110.4$ K for air. The viscosity temperature exponent was defined as

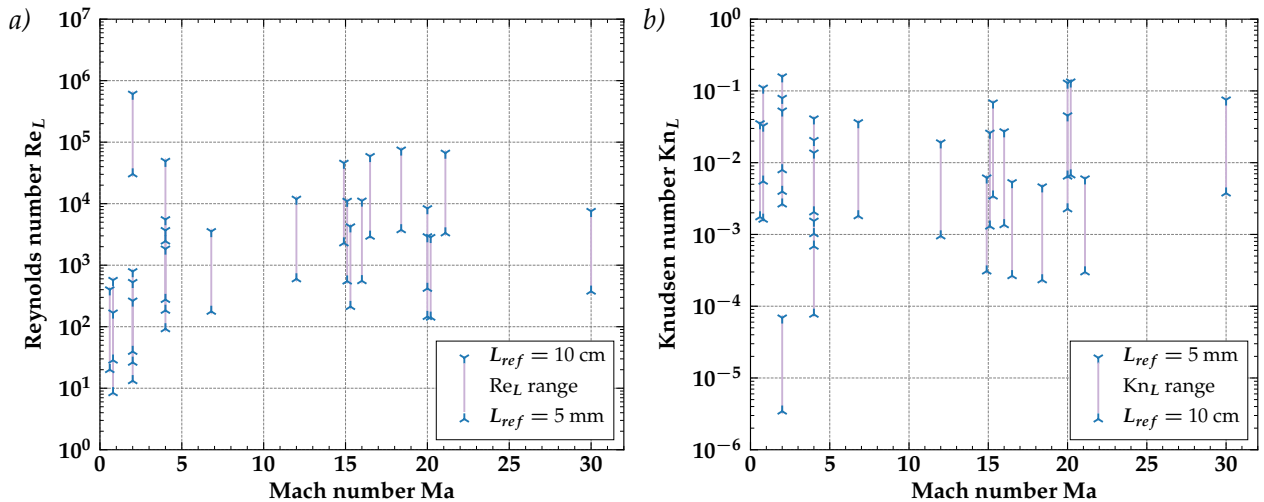$$\omega = 1.5\frac{T}{B + T}.$$ (4)

Figure 3: Flow conditions of the MARHy wind tunnel in terms of: *a)* Reynolds number, and *b)* Knudsen number. The flow condition of each available nozzle is represented in terms of range obtained with two extreme reference lengths: 5 mm and 10 cm.

2.3 Diagnostics

Different types of experimental diagnostics were used to characterize the flow topology around the models tested in the MARHy wind tunnel.

Pressure measurements: The Mach 4 air flow was set by the difference between the settling chamber pressure and the test chamber pressure. To ensure an accurate operating mode during experiments, the pressure parameters of the wind tunnel were continuously acquired with absolute capacitive sensors whose scales are adapted to the range of the measurement values expected. Specially the stagnation pressure p_0 and test section pressure p_∞ were measured with two MKS Baratron capacitance manometers (Type 627D) with 0–10 Torr and 0–0.01 Torr ranges, respectively. Both manometers are connected to a MKS control unit (PR 4000B) with a 12-bit resolution.

Shock wave visualization: The flow around the tested model was visualized with a Kuro CMOS Cameras (2048 × 48-pixel array) with back-illuminated technology, equipped with a VUV objective lens (94 mm, $f/4.1$). The light was collected through a fluorine window located in the wall of the test section chamber.[2] Due to the rarefaction level of the flow, the flow field around the model was experimentally visualized through the rarefied flow visualization technique. This technique allows shock waves to be distinguished in low density flows, where other techniques, for instance, Schlieren cannot be applied because of the low density of the flow. The rarefied flow visualization technique consists in using an electric discharge to weakly ionize the air flowing around a model in the test chamber. In this study, a negative voltage (ranged between −750 V and −1.7 kV) was applied between two parallel rectangular copper plates separated by a gap of about 350 mm. The tested model was placed between these large electrodes, leading to a stream of ionized air around the model. The consecutive diffuse light emission was focused on the CMOS camera. Due to air density variations in the shock wave, a change in the light intensity in the resulting picture allowed the shock wave to be detected.[2]

Surface temperature measurements: The evolution of the surface temperature of the model placed within the supersonic flow was monitored with an infrared thermography device. The surface temperature was measured with an OPTRIS PI 400 camera, which has a spectral range lying between 7.5 μm and 13 μm. The IR camera was placed on top of the wind tunnel and focused the entire surface of the flat plate through a ZnSe window. The viewing angle remained unchanged throughout the experiments. The lens used in this study was a O13 Telephoto lens with an aperture of 13° × 10° (FOV) with an image resolution of 0.61 mrad (IFOV). The IR detector covers a surface of 382 × 288 pixels and the focus length between the model surface and the IR camera was 1395 mm ± 10 mm. This corresponded to a spatial resolution of 0.84 mm pixel^{-1} ± 0.01 mm pixel^{-1} in the focus plane, along both X (in the longitudinal direction) and Y (in the transverse direction) axes. Focusing of the IR camera was performed before each run of the wind tunnel by placing a heated coin (head side) on the flat plate surface. The models tested in the wind tunnel were painted with a high temperature flat black paint to obtain a surface emissivity higher than 0.8. This ensured a minimal deviation from the black body temperature (considered for the model surface by the IR camera) given the experimental set-up of the present study.[2] The post-processing technique used to asses the actual temperature of the surface model is detailed in Joussot *et al.*(2015).

2.4 Models

Three different types of models were tested in the MARHy wind tunnel: 1U, 2U, and 3U CubeSat; a simplified model of the Chinese space station Tiangong-1; and a model geometry similar to the IXV (namely, the "IXV-like model" in this paper).

CubeSat: The term CubeSat is used to describe a small satellite, which is build with basic unit cubes of 10 cm-edge ("1U" blocks). CubeSat units can be assembled together to form bigger satellites with the most used configuration being 3U (about 64%), followed by 1U (18%), then 6U.[7] In the present study, three different CubeSat configurations were studied: 1U, 2U, and 3U. Each simplified model of CubeSat tested in the wind tunnel was composed of two parts: a body made of Macor with a reference edge of 10.25 mm, and solar panels cut in a semi-rigid metal plate. To respect the CubeSat design specification, the thickness of solar panels was 0.3 mm. The simplified models of 1U, 2U, and 3U had therefore a total length of 10.25 mm, 20.50 mm, and 30.75 mm, respectively. Each model of CubeSat was painted in flat black for the surface temperature measurements (Fig. 4). The reference dimension for the Reynolds number and the Knudsen number were based on the 1U edge of 10.25 mm. Figure 5 shows the comparison between the EntrySat CubeSat trajectory[5,6] and the flow conditions of the MARHy wind tunnel. The red open circle corresponds to the experimental free stream conditions of the present study (see Tab. 1).

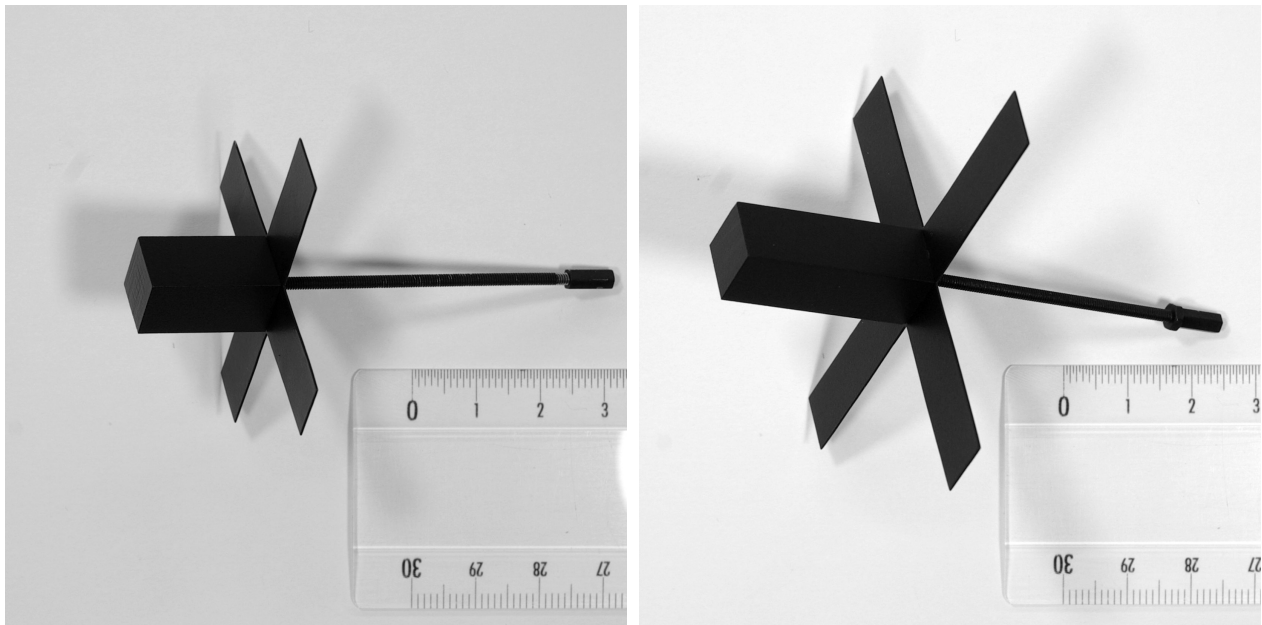EXPERIMENTAL STUDY OF FLOW FIELD AROUND HYPERSONIC VEHICLE AND RE-ENTERING SPACECRAFT

Figure 4: Pictures of the CubeSat model: 2U configuration (left panel), and 3U configuration (right panel).

Tiangong-1:

IXV-like:

3. Results

3.1 CubeSat models

3.2 Tiangong-1 model

3.3 IXV-like model

4. Conclusions

5. Acknowledgments

References

[1] W H Ailor and R P Patera. Spacecraft re-entry strategies: meeting debris mitigation and ground safety requirements. *Proceedings of the Institution of Mechanical Engineers, Part G: Journal of Aerospace Engineering*, 221(6):947–953, 2007.

[2] R Joussot, V Lago, and J-D Parisse. Quantification of the effect of surface heating on shock wave modification by a plasma actuator in a low density supersonic flow over a flat plate. *Experiments in Fluids*, 56(5):102, 2015.

[3] V Lago, E Depussay, P Lasgorceix, A Lebéhot, and J-P Martin. The experimental facilities at Laboratoire d'Aérothermique. *AIP Conference Proceedings*, 762:1337–40, 2005.
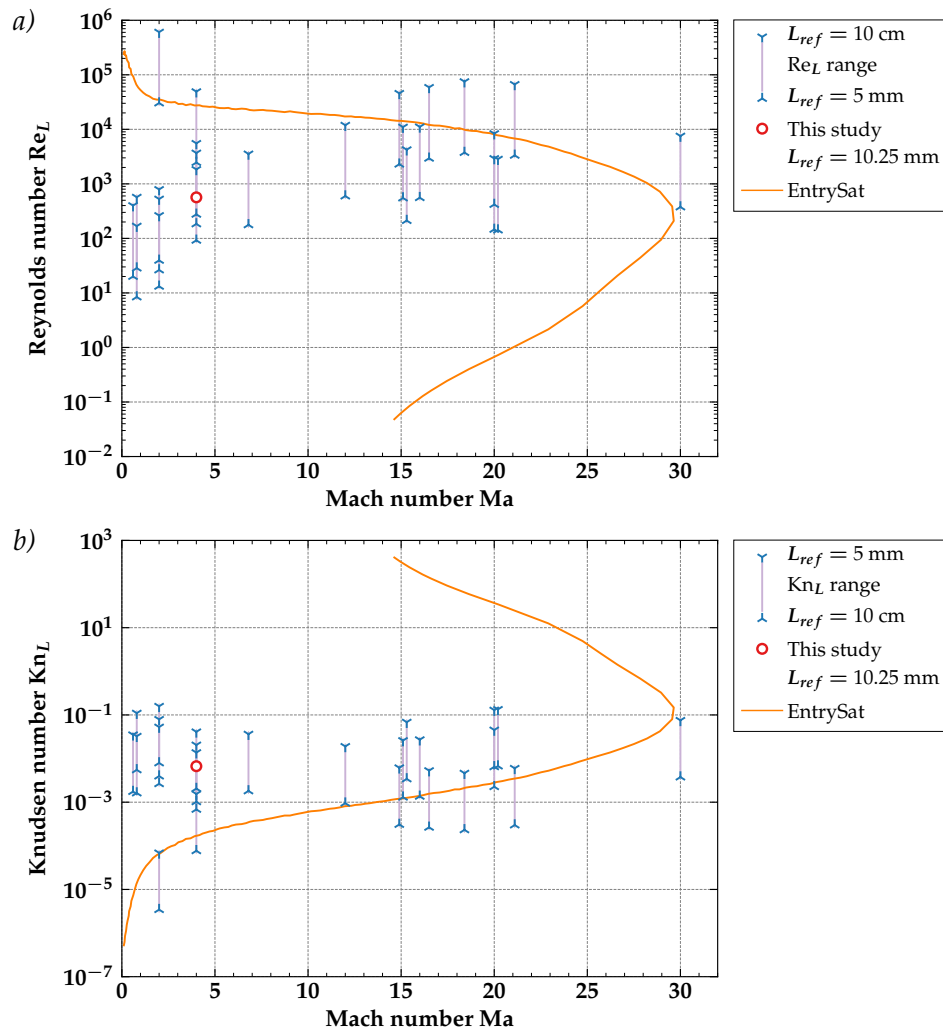
Figure 5: Comparison of EntrySat re-entry trajectory[5] and flow conditions of the MARHy wind tunnel: *a)* Mach-Reynolds diagram, and *b)* Mach-Knudsen diagram.

[4] J M Picone, A E Hedin, D P Drob, and A C Aikin. NRLMSISE-00 empirical model of the atmosphere: Statistical comparisons and scientific issues. *Journal of Geophysical Research: Space Physics*, 107(A12):SIA 15–1–SIA 15–16, 2002.

[5] Y Prevereaud, F Sourgen, D Mimoun, A Gaboriaud, J-L Verant, and J-M Moschetta. Predicting the atmospheric re-entry of space debris through the QB50 EntrySat mission. In *6th European Conference on Space Debris (ESA SP-723), Darmstadt, Germany, 22-25 April, 2013*, pages 1–7, 2013.

[6] F Sourgen, Y Prévereaud, J-L Vérant, E Laroche, and J-M Moschetta. MUSIC/FAST, a pre-design and pre-mission analysis tool for the Earth atmospheric re-entry of spacecraft capsules and de-orbited satellites. In *8th European Symposium on Aerothermodynamics for Space Vehicles, Lisbonne, Portugal, 2-6 March 2015*, pages 1–10, 2015.

[7] T Villela, C A Costa, A M Brandão, F T Bueno, and R Leonardi. Towards the thousandth CubeSat: A statistical overview. *International Journal of Aerospace Engineering*, 2019:5063145 (13 pp.), 2019.